COHERENT PHOTOPRODUCTION OF J/Ψ AND HIGH-MASS e^+e^- PAIRS IN ULTRA-PERIPHERAL AU+AU COLLISIONS AT $\sqrt{s_{NN}}$ = 200 GeV

David d'Enterria
for the PHENIX Collaboration
Nevis Labs, Columbia University, Irvington, NY 10533, and New York, NY 10027, USA
LLR, Ecole Polytechnique, 91128 Palaiseau, France, EU

High energy ultra-peripheral collisions (UPC) of heavy-ions generate strong electromagnetic fields which open the possibility to study γγ and γ-nucleus processes in a kinematic regime so far unexplored. We report on preliminary PHENIX results of J/ψ and high-mass e^+e^- photoproduction at mid-rapidity in coherent electromagnetic Au+Au interactions at $\sqrt{s_{NN}}$ = 200 GeV tagged with forward neutron emission from the $Au^\star$ dissociation.

1 INTRODUCTION

1.1 γγ, γp physics at e^+e^- and ep colliders

Our knowledge about elementary particles and their fundamental interactions is mainly obtained through the study of high energy particle collisions. A part from the more "conventional" e^+e^-, ep (DIS) and pp, $\bar{p}p$ collisions, high-energy γγ [1] and γp [2] processes provide an interesting and complementary approach to study strong and electro-weak interactions. At high energies, a (quasi) real photon can interact as a point-like particle (e.g. Compton-like scattering) or through quantum fluctuations into a charged-fermion pair ($q\bar{q}$, l^+l^-), a charged-boson pair (e.g. W^+W^-) or directly into a vector meson (carrying the same quantum numbers $J^{PC} = 1^{--}$ as the photon). At energies below the W^+W^- threshold, the photon wave function can be written as [2]

$$|\gamma\rangle = c_0\,|\gamma_0\rangle \;+\; \sum_{V=\rho,\omega,\phi,J/\psi,\Upsilon} c_V\,|V\rangle \;+\; \sum_{q=u,d,s,c,b} c_q\,|q\bar{q}\rangle \;+\; \sum_{l=e,\mu,\tau} c_l\,|l^+l^-\rangle. \qquad (1)$$

Though in practice the first term dominates (i.e. $c_0 \approx 1$), hadronic/partonic fluctuations (under the non-perturbative "Vector-Dominance-Model" form $\gamma \rightarrow V$ or, at larger $q\bar{q}$ virtualities, via "resolved" quark pairs $\gamma \rightarrow q\bar{q}$ which can, at their turn, radiate also gluons) interact strongly and give the largest contribution to the total γγ, γp cross-sections at high energies. Fig. 1 shows the total hadronic cross-sections measured in e^+e^-, γγ and γp collisions as a function of the center-of-mass energy $\sqrt{s}$. While, the (s-channel) e^+e^- annihilation cross-section decreases with increasing energy ($\sigma_{ee\rightarrow hadrons} \propto \alpha_{em}^2/s$), photon-induced collisions behave like pp, $p\bar{p}$ collisions. Their cross-sections rise monotonically with $\sqrt{s}$ in agreement with an increasingly large Pomeron (or two-gluon) exchange contribution as described by Regge phenomenology [3, 4]. Although in the present-day there are no beams of high energy *real* photons available, beams of high energy *quasi-real* or *virtual* photons are commonly generated at e^+e^- and ep colliders. Indeed, the
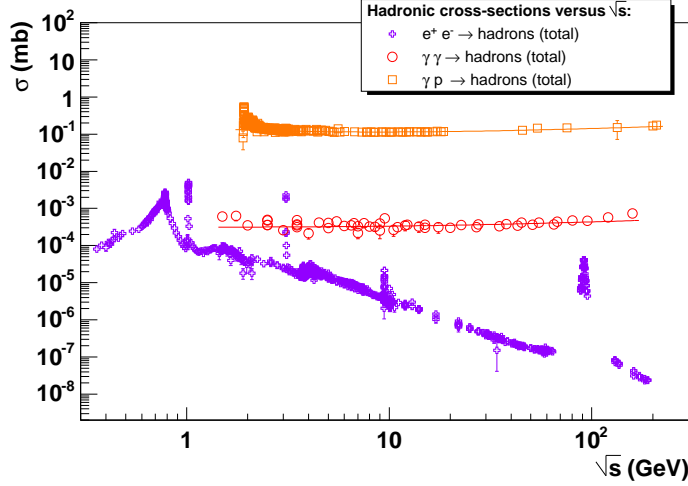
Fig. 1. Total hadronic cross-section in e^+e^-, $\gamma\gamma$ and γp collisions as a function of the center-of-mass energy $\sqrt{s}$. The data is from the PDG [5], and the fits to $\gamma\gamma$, γp data are the latest Regge-theory parametrizations of the COMPETE collaboration [4].

electromagnetic field of any relativistic charged particle can be described as a flux of "equivalent" photons with energy distribution $f_{\gamma/e}(z) = dN_\gamma/d\omega$ given by the Weizsäcker-Williams [6] or Equivalent Photon Approximation (EPA) formula, which for an $e^\pm$ beam reads:

$$\frac{dN_\gamma}{dz} \approx \frac{\alpha_{em}}{2\pi}\frac{1}{z}[1+(1-z)^2]\ln\frac{Q^2_{max}}{Q^2_{min}} \quad , \text{ with } \quad z = \omega/E_e. \tag{2}$$

Here z is the fraction of the $e^\pm$ energy carried by the photon and $Q^2 = -(q^2)$ the γ virtuality. $Q^2_{min} = m_e^2 z^2/(1-z) \approx 0$ GeV$^2/c^2$, whereas Q^2_{max} depends on the properties of the produced X, e.g. $Q^2_{max} \approx m_\rho^2$ for hadron production, and $Q^2_{max} \approx W^2$ for $X = l^+l^-$, where $W^2 = W^2_{\gamma\gamma} = 4\omega_1\omega_2$ (or $W^2 = W^2_{\gamma p} = 4E_p E_e z$) is the squared $\gamma\gamma$ (or γp) c.m. energy. Fig. 2 shows the typical two-photon ($e^+e^- \to e^+e^-\gamma\gamma \to e^+e^-X$) and photon-proton ($ep \to e\gamma p \to epX$) processes commonly studied at LEP and HERA colliders. Two basic properties characterize $\gamma\gamma$ and γp collisions:

- The variable-energy photon "beam" always carries less energy than the parent lepton beam (the spectrum (2) has a soft bremsstrahlung shape, $dN_\gamma/d\omega \propto ln(1/\omega)/\omega$, peaked at low ω) and thus the available center-of-mass energies are typically $0.1\sqrt{s} \lesssim W_{\gamma\gamma,\gamma p} \lesssim 0.5\sqrt{s}$.

- The (almost) real photons beams have, by definition, $Q^2 \approx 0$ (they are often kinematically selected by requiring the scattered parent $e^\pm$ to be close to the incident direction) and thus the produced X have always small transverse momentum (at variance with DIS scattering where the $\gamma^\star$ has $Q^2 \gtrsim 2$ GeV$^2/c^2$ and the produced particles have large p_T).

The main interest of γ-induced processes at e^+e^-, ep colliders so far is that they allow for precision studies of QCD dynamics (tests of Regge theory, low-energy quark model spectroscopy, BFKL evolution, hard-scattering factorization, diffractive interactions, ...) in a background-free environment and with a comparatively simpler initial state than in hadron-hadron collisions. QED processes (e.g. l^+l^- production), on the other hand, have been less addressed than QCD-related studies. Typical physics measurements encompass [7]: (i) total hadronic cross-sections, (ii) $\gamma\gamma$ widths ($\Gamma_{\gamma\gamma}$) of C-even (scalar $0^{-+,++}$ and tensor $2^{++,\cdots}$) mesons, (iii)
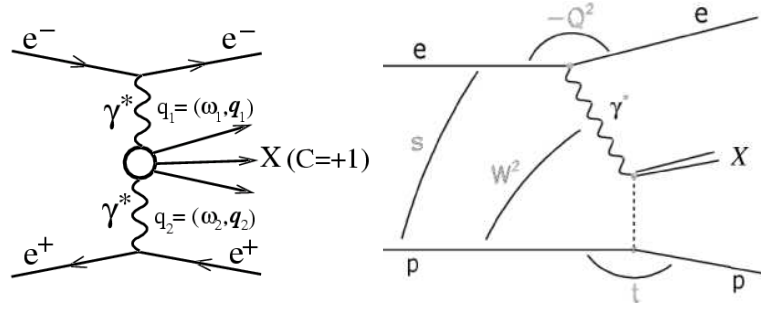
Fig. 2. Typical diagrams for photon-photon (left) and photon-proton (right) reactions at e^+e^- and ep colliders respectively.

double vector meson production ($\rho, \omega, \phi, J/\psi, \Upsilon$), (iv) structure function of the photon, (v) (hard) photo-production of quarkonia ($J/\psi, \Upsilon$), open heavy quarks and jets; and (vi) diffractive structure functions. The corresponding two-photon ($\sigma_{\gamma\gamma \to X}$) or photo-production ($\sigma_{\gamma p \to X}$) cross-sections are theoretically computed using different methods depending on the c.m. energy W and the nature of the produced particle X. Regge-based models (as e.g. in the DPM [8]), (Generalized) Vector-Meson-Dominance (VDM) approaches [9], pQCD factorization [10] (with different available parametrizations of the parton distribution function of the photon [11]), color-dipole (or saturation) approaches [12, 13], or a combination (of some) of them (as e.g. in PHOJET [14] or PYTHIA [2] event generators) are often used.

At future linear collider facilities using beams of back-scattered laser photons off beam electrons, new prospects appear both within the Standard Model (Higgs production, triple gauge couplings, precision top physics) and beyond-SM (SUSY particle production, extra-dimensions, ...) [15].

1.2 $\gamma\gamma$, γA physics in ultra-peripheral A+A reactions

As aforementioned, any relativistic charged particle generates a flux of quasi-real photons which can be used for photoproduction studies. Though in the previous Section we have considered the case of $e^\pm$ beams, the same holds obviously true for accelerated protons [16] or nuclei [17,18,19]. The corresponding Equivalent Photon Approximation formula (2) for an extended object such as a proton or a nucleus with charge Z and mass m_A is [1]

$$f_{\gamma/A}(z) = \frac{\alpha_{em} Z^2}{2\pi} \frac{1+(1-z)^2}{z} \int_{Q^2_{min}}^{\infty} \frac{Q^2 - Q^2_{min}}{Q^4} |F(Q^2)|^2 dQ^2, \qquad (3)$$

where Q^2 is the momentum transfer from the projectile, $Q^2_{min} = m_A^2 z^2/(1-z)$, and $F(Q^2)$ a nuclear form factor describing its spatial distribution. From Eq. (3) one can see that the equivalent photon flux in relativistic heavy-ion collisions (with charge $Z \sim 80$ for conventional Au or Pb beams) has an amplification factor of $Z^2 \sim 6.5 \cdot 10^3$ compared to $e^\pm$ or proton beams. The corresponding $\gamma\gamma$ cross-sections are a factor $Z^4 \sim 4 \cdot 10^7$ larger ! This fact drives the main interest on coherent electromagnetic (or ultra-peripheral) interactions of heavy-ions [17, 18, 19]. For collisions between heavy-ions, rather than Eq. (3) it is more useful the expression for the equivalent photon spectrum above a given minimum impact parameter [20] which is usually chosen as twice the nuclear radius, $b > b_{min} \approx 2 R_A$ (i.e. $b_{min} \approx 15$ fm for Au, Pb beams), so that the contribution from non-electromagnetic ion-ion interactions can be removed:

$$f_{\gamma/A}(z, b > b_{min}) = \frac{\alpha_{em} Z^2}{\pi} \frac{1}{z} \left[2x K_0(x) K_1(x) - x^2 \left(K_1^2(x) - K_0^2(x) \right) \right], \qquad (4)$$

where $K_{0,1}$ are the modified Bessel functions of the 2nd kind and $x = z m_A b_{min}$. The validity of the application of the EPA formula for heavy-ions is limited to the case where *all* the protons of the nucleus interact electromagnetically in a coherent way. In that case, the wavelength of the resulting photon is larger than the size of the nucleus, given by its radius R_A. This "coherence" condition limits the maximum virtuality of the produced photon to very low values [17]:

$$Q^2 = \left(\omega^2/\gamma^2 + q_\perp^2\right) \lesssim 1/R_A^2 \quad \text{(where } \gamma \text{ is the beam Lorentz factor)}, \tag{5}$$

and thus for most purposes (but for lepton pair production) those photons can be considered as (quasi) real with maximum energy and perpendicular momentum:

$$\omega < \omega_{max} \approx \frac{\gamma}{R} \quad, \text{ and } q_\perp \lesssim \frac{1}{R} \approx 30\,\text{MeV}. \tag{6}$$

At RHIC (LHC) energies with $\gamma = 100$ ($\gamma \approx 2800$ for Pb), the maximum photon energy in the lab system is $\omega_{max} \approx 3$ GeV (80 GeV). Thus, the corresponding maximum energies in the c.m. system for $\gamma\gamma$ and γA processes are $W_{\gamma\gamma}^{max} \approx 6$ (160) GeV and $W_{\gamma A}^{max} \approx 34$ (940) GeV respectively.

1.3   Production cross-sections in UPC collisions

The production cross-section of a system X in UPC A+A collisions is computed as the convolution of the corresponding equivalent photon spectrum (4) with the elementary photonuclear or two-photon cross-sections:

$$\sigma(A + A \rightarrow \gamma + A + A \rightarrow A + A + X) = \int_0^1 f_{\gamma/A}(z)\sigma_{\gamma A \rightarrow X}(W_{\gamma A})dz \tag{7}$$

$$\sigma(A + A \rightarrow \gamma\gamma + A + A \rightarrow A + A + X) = \int_0^1 \int_0^1 f_{\gamma/A}(z_1)f_{\gamma/A}(z_2)\sigma_{\gamma\gamma \rightarrow X}(W_{\gamma\gamma})dz_1 dz_2 \tag{8}$$

where, as aforementioned, the elementary $\sigma_{\gamma A \rightarrow X}$ and $\sigma_{\gamma\gamma \rightarrow X}$ are theoretically computed using different methods depending on the c.m. energy W and the particle X. The two cases of interest in this paper, shown in Figure 3, are the coherent photoproduction of:

I. J/ψ, the heaviest vector meson effectively accessible in γA collisions at RHIC, via:
   $A + A\,(\rightarrow \gamma + A) \rightarrow A^\star + A^{(\star)} + J/\psi$.

II. High mass di-electron continuum in $\gamma\gamma$ collisions: $A + A\,(\rightarrow \gamma + \gamma) \rightarrow A^\star + A^{(\star)} + e^+ + e^-$.

For the first process (I), $\sigma_{\gamma A \rightarrow J/\psi A}$ has been determined using perturbative QCD for the $\gamma p \rightarrow J/\psi p$ process [21] plus initial-state shadowing and final-state J/ψ-nucleus interaction [22], or within the color-dipole formalism [13]. The cross-section for heavy vector meson ($J/\psi, \Upsilon$) photoproduction is found to depend (i) *quadratically* on the gluon density $G_A(x, Q^2)$ [23]:

$$\frac{d\sigma(\gamma A \rightarrow V A)}{dt}\bigg|_{t=0} = \frac{\alpha_s^2 \Gamma_{ee}}{3\alpha M_V^5}16\pi^3 \left[x G_A(x, Q^2)\right]^2 \quad, \text{ with } Q^2 = M_V^2/4 \quad, \text{ and } x = M_V^2/W_{\gamma A}^2, \tag{9}$$

as well as on (ii) the probability of rescattering or absorption of the $Q\overline{Q}$ pair as it traverses the nucleus. The study of quarkonia production in γA collisions at RHIC or LHC energies is, thus, considered an excellent probe of (i) the gluon distribution function $G_A(x, Q^2)$ in nuclei, and (ii) vector-meson dynamics in nuclear matter.

For the second purely electromagnetic process (II), the total $\sigma_{\gamma\gamma \rightarrow \gamma\gamma e^+ e^-}$ cross-section is huge (about 30 kb for Au+Au at RHIC !) but strongly peaked at forward-backward rapidities and
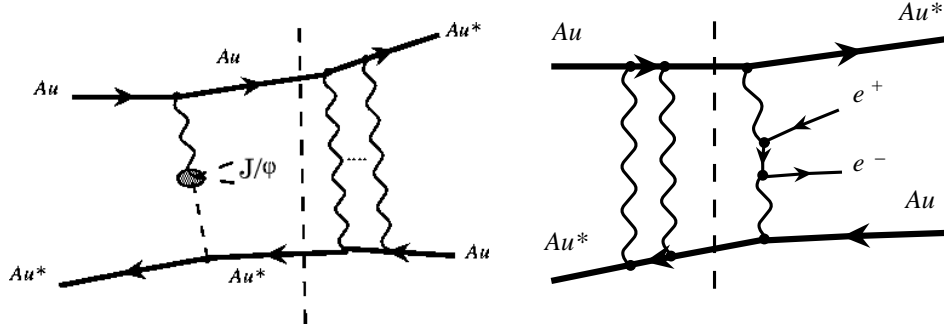
Fig. 3. Lowest order Feynman diagrams for J/ψ (left) and dielectron pair (right) production in $\gamma\gamma$ and γA processes accompanied by Au Coulomb excitation in ultra-peripheral Au+Au collisions.

at low $m_{inv} \lesssim 10\,\text{MeV}/c^2$ [17]. Several calculations exist for multiple $e^\pm$ pair production within QED [17] or solving the semi-classical Dirac equation [24]. The main interest of such coherent $\gamma\gamma$ collisions is that one can test QED in a very strong field regime ($Z\alpha_{em} \approx 0.6$) where perturbative calculations are expected to break [25].

2   EXPERIMENTAL

At RHIC energies, the production cross section for vector mesons (ρ, ϕ, J/ψ, Υ) in UPC Au+Au is large and accounts for as much as $\sim$10% of the total $\sigma_{AuAu} \approx 7$ b nuclear cross section [26,27]. Measurements of coherent photonuclear production of the ρ meson [28] as well as $\gamma\gamma$ production of *low-mass $e^\pm$* pairs [29] have been performed by the STAR collaboration. The PHENIX analysis presented here aims at similar measurements but at higher invariant masses.

Detailed knowledge of the experimental signatures of coherent UPC events is a basic pre-requisite to setup an efficient UPC trigger and to define the reconstruction and analysis cuts used in the present work. The typical characteristics of UPC Au+Au events are:

1. Low central multiplicities: typical values are (well) below $\sim$15 particles.

2. Low total transverse momentum ("coherence condition"): $p_T < 2\hbar c/R \approx 50$ MeV/c or $p_T \sim m_{inv}/\gamma \approx 30$ MeV/c.

3. Large probability of multiple electromagnetic interactions (γ-exchanges shown in Fig. 3) leading to (single or double) nucleus Giant-Dipole-Resonance (GDR) excitation followed by Xn neutron(s) decay. Typical probabilities are $P_{1n} \sim$30-50% (J/ψ) or $P_{1n} \sim$20% (ρ) which factorize out when determining the UPC cross-sections [25, 30].

4. Zero net charge: even number of charged tracks of opposite signs.

5. Narrow dN/dy peaked at mid-rapidity (narrower for larger m_{inv}).

Property 3. is the most useful for UPC tagging and trigger purposes.

2.1   PHENIX setup and luminosity

The data presented here were collected with the PHENIX detector at BNL RHIC during the 2004 high luminosity Au+Au run at $\sqrt{s_{NN}} = 200$ GeV (Run-4). The gold beams had 45 or 56 bunches

with 10^9 ions/bunch and 106 ns crossing-time. Typical luminosities at the beginning of the store were $\sim 2\ 10^{26}$ cm^{-2}s^{-1}, twice larger than the design luminosity (thanks mainly to an improved vacuum system) [31]. The PHENIX detector [32] is specifically designed to measure hard probes by combining good mass and particle identification (PID) resolution in a broad momentum range, high rate capability, and small granularity. The central-arm detectors used in this analysis (DC, PC, RICH and EMCal) are those needed for the measurement of J/ψ (e^+e^- decay mode) and high-mass ($m_{inv} > 2$ GeV/c^2) dielectron pairs at $y = 0$. The ultra-peripheral Au+Au events were tagged by neutron detection at small forward angles in the Zero-Degree-Calorimeters (ZDC).

The momentum and trajectory of the tracks were reconstructed with the central tracking (CNT) system (covering $\Delta\eta = 0.7$ and $\Delta\phi = \pi$) based on a multi-layer drift chamber (DC) followed by multi-wire proportional chambers (PC) with pixel-pad readout, both placed in an axial magnetic field parallel to the beam ($B_{max} = 1.15$ T m). Electron-positron identification was done with the Ring-Imaging- Čerenkov (RICH, with CO_2 gas radiator) and electromagnetic calorimeter EM-Cal [33], with a total total solid angle at mid-rapidity of $\Delta\eta \approx 0.7$ and $\Delta\phi = \pi$. The PHENIX EMCal consists of six sectors of lead-scintillator sandwich calorimeter (PbSc, 15552 individual towers with 5.54 cm $\times$ 5.54 cm $\times$ 37.5 cm, $18X_0$) and two sectors of lead-glass Čerenkov calorimeter (PbGl, 9216 modules with 4 cm $\times$ 4 cm $\times$ 40 cm, $14.4X_0$), at a radial distance of ~ 5 m from the beam line. The ZDC [34, 35] hadronic calorimeters placed 18 m up- and downstream of the interaction point, cover the very-forward region, $|\theta| < 2$ mrad, and measure the energy of the neutrons coming from the Au* Coulomb dissociation, with $\sim 20\%$ resolution.

The total equivalent sampled luminosity for this study was: $\mathcal{L}_{int} = N_{BBC-LL1}/\sigma_{AuAu} \times \varepsilon_{BBC} = 120 \pm 10\ \mu$b^{-1}, where $N_{BBC-LL1} = 886 \cdot 10^6$ is the total number of events collected (after vertex cut and QA) by the Beam-Beam-Counter (BBC) minimum bias Au+Au trigger, and we use for this preliminary analysis the "nominal" values for the Au+Au total cross-section ($\sigma_{AuAu} = 6.85$ b) and BBC-LL1 trigger efficiency ($\varepsilon_{BBC} = 92 \pm 3\%$) [36].

2.2   Trigger and data sample

The events used in this analysis were collected by a level-1 UltraPeripheral (LL1-UPC) trigger set up for the first time in Run-4, with the following characteristics:

1. Veto on coincident signals in both BBC (covering $3.0 < |\eta| < 3.9$ and full azimuth) is imposed in order to reduce peripheral nuclear and beam-gas collisions.

2. A large energy ($E > 0.8$ GeV) cluster in EMCal is required to select the $e^\pm$ from the J/ψ decay ($E \approx 0.5\,m_{J/\psi} \approx 1.6$ GeV) and from the high-mass di-electron continuum.

3. At least 30 GeV energy deposited in one or both of the ZDCs is required to select Au+Au events with forward neutron emission (Xn) from the (single or double) Au* decay.

The trigger used to detect high-energy electrons in the central arm was the standard EMCal-RICH-Trigger (ERT) with 2×2 tile threshold at 0.8 GeV. A software algorithm performed a crude reconstruction of EMCal clusters by summing the pedestal-subtracted and gain-calibrated energies in overlapping "tiles" of 2×2 calorimeter towers with an estimated (preliminary) efficiency for high-energy $e^\pm$ coming from the J/ψ decay of $\varepsilon_{trigg}^{J/\psi} = 0.9 \pm 0.1$.

The total number of events collected by the UPC trigger was 8.5 M (i.e. 0.4% of the min.bias Au+Au trigger) and the data set comprised ~ 1000 raw-data files (~ 1. TB). Standard QA further

reduced this number down to 6.7 M events. Most of these UPC-triggered events were not, however, signals of interest in this analysis (*coherent J/ψ* and high-m_{inv} e^+e^-). Other events (with their discriminating characteristics indicated) were likely to fire also the UPC trigger [17,18,19]:

(1) Cosmic rays: no ZDC, no good vertex.

(2) Beam-gas collisions: no good vertex, large multiplicity, asymmetric dN/dy.

(3) Peripheral nuclear collisions: comparatively large particle multiplicities, large pair p_T.

(4) (Hard) diffractive collisions: Pomeron-Pomeron events with rapidity gap(s) [37, 38] are usually accompanied by forward proton emission, $p_T(I\!\!PI\!\!P) > p_T(\gamma\gamma)$, and like-sign pairs.

(5) Coherent $\gamma\gamma \to q\bar{q}$: produce mainly hadrons (removable by the $e^{\pm}$ identification cuts).

(6) Incoherent (or "quasi-elastic") photon-nucleon (γN) collisions: $p_T(\gamma I\!\!P) > p_T(\gamma\gamma)$, wider and asymmetric dN/dy, $Xn \geq 2n$ (recoiling nucleon induces nuclear break-up with larger probability than in fully coherent interactions) [22].

Processes (1) and (2) can be considered "non-physical" sources of background and are rejected by simple global event analysis cuts. "Physical" processes (3), (4), (5) can be removed by offline cuts more easily than the γN contribution (6) which has experimental signatures very similar to true γA reactions (see [22] and Section 3.3).

2.3   Data analysis

Charged particle tracking in PHENIX central arms is based on a combinatorial Hough transform in the track bend plane, with the polar angle determined by PC1 and the collision vertex along the beam direction [39]. The original *z*-vertex of the track was measured with 1-cm resolution using a specific method based on PC hits and EMCal clusters since the standard procedure based on BBC and ZDC is not applicable for UPC events which, by definition, do not have BBC coincidences and often do not have ZDC coincidences. Track momenta are measured with a resolution $\delta p/p \approx 0.7\% + 1.0\% \, p \approx 1.7 - 2.7\%$ for the relevant range ($p \sim 1 - 3\,GeV/c$) in this analysis.

The following global cuts were applied to enhance the sample of genuine γ-induced events:

1. A standard offline vertex cut $|vtx_z| < 30$ cm was required to select collisions well centered in the fiducial area of the central detectors and to avoid tracks close to the magnet poles.

2. The maximum event multiplicity allowed was 15 tracks to suppress the contamination of non-UPC (mainly beam-gas and peripheral nuclear) reactions that fired the UPC trigger.

At variance with standard $J/\psi \to e^+e^-$ analyses in nuclear Au+Au reactions [40] which have to deal with large particle multiplicities, we did not need to apply very strict PID cuts in order to identify electrons in the clean UPC environment:

1. RICH multiplicity $n_0 \geq 2$ selects $e^{\pm}$ which fire 2 or more tubes separated by the nominal ring radius.

2. Good CNT–EMCal matching is required for candidate tracks with an associated EMCal cluster without dead-warn towers within a 2×2 tile.

3. An EMCal cluster energy cut ($E_1 > 1$ GeV $||$ $E_2 > 1$ GeV) is applied to select candidate $e^{\pm}$ in the plateau region above the turn-on curve of the ERT trigger (with 0.8 GeV threshold).

Beyond those global or single-track cuts, an additional "coherent" identification cut was applied by selecting only those e^+e^- candidates detected in opposite arms ($arm_1 \neq arm_2$). Such a cut enhances the sample of back-to-back di-electrons with low pair p_T as expected for $\gamma\gamma$, γA production. Finally, J/ψ were reconstructed by standard invariant mass analysis of all $e^\pm$ that passed the aforementioned analysis cuts. Any remaining background was removed from the m_{inv} distribution by directly subtracting the wrong sign pairs (e^+e^+ or e^-e^-) from the unlike-sign pairs in a *bin-to-bin basis*. The J/ψ yield is extracted directly by adding the number of counts within $\pm 3\sigma$ (roughly $2.7 - 3.5$ GeV/c^2) of a Gaussian fit of the experimental mass peak.

2.4 Acceptance and efficiency corrections

Physical cross-sections are obtained after correcting the raw number of signal counts for: (i) the geometrical acceptance of our detector system, and (ii) the efficiency losses introduced by the aforementioned analysis cuts. Acceptance and efficiency corrections were obtained with a full Monte Carlo of the experimental apparatus with realistic input distributions of the physical signals. We generated 10^5 events for each one of the two coherent process of interest: J/ψ and high-mass e^+e^- pairs production in Au+Au collisions accompanied by Xn forward emission, with the *Starlight* Monte Carlo [26, 27, 41]. Such a model reproduces well the existing $d^3N/dyd\phi dp_T$ distribution of coherent ρ production in UPC Au+Au events measured at RHIC by STAR [28]. The coherent events were simulated in the PHENIX detector using GEANT [42] and passed through the same reconstruction program as the real data. Figure 4 shows, for illustrative purposes, the invariant mass dN/dm_{ee} distributions of the coherent J/ψ's and e^+e^- signals given by *Starlight* and a *fast* Monte Carlo version of our code [41]. A Gaussian J/ψ signal is expected with experimental width of $\sim$100 MeV/c^2 at $m_{inv} \sim 3.1$ GeV/c^2 on top of a power-law-like e^+e^- continuum. The J/ψ correction factors obtained from our simulation studies are:

1. Acceptance ($J/\psi \rightarrow e^+e^-$ decay detected within $|y| < 0.5$ and full ϕ): $Acc = 5.7\%$.

2. Efficiency losses due to all cuts (including yield extraction within $\pm 3\sigma$): $\varepsilon_{reco} = 56.4\%$.

3. Unlike-sign background subtraction results in a negligible efficiency loss of the J/ψ signal.
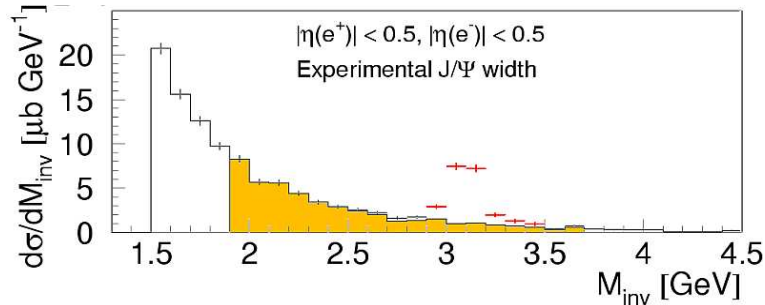

Fig. 4. Expected invariant mass distribution of dielectron pairs from $\gamma A \rightarrow J/\psi \rightarrow e^+e^-$ (red points) and $\gamma\gamma \rightarrow e^+e^-$ (histogram) as given by the *Starlight* model [41] for UPC Au+Au collisions at $\sqrt{s_{NN}} = 200$ GeV detected in PHENIX. The hatched area indicates the region accessible with our ERT trigger.

3 EXPERIMENTAL RESULTS

Fig. 5 left, shows the invariant mass of unlike-sign pairs (red-filled histogram) and same-sign background pairs (yellow-filled histo) obtained from our analysis after application of the global,

single and pair cuts described in the previous section. The wrong-sign background is very small as expected from the MC results and has a flat p_T distribution which extends far from the low-p_T coherent region (Fig. 5 right). In what follows, all (m_{inv} and dN/dp_T) distributions have the like-sign background removed. Note that below $m_{inv} \approx 1.8$ GeV/c^2, the applied offline cuts above the ERT threshold energy ($E_{1,2} > 1$ GeV) are responsible for the effective lack of counts.
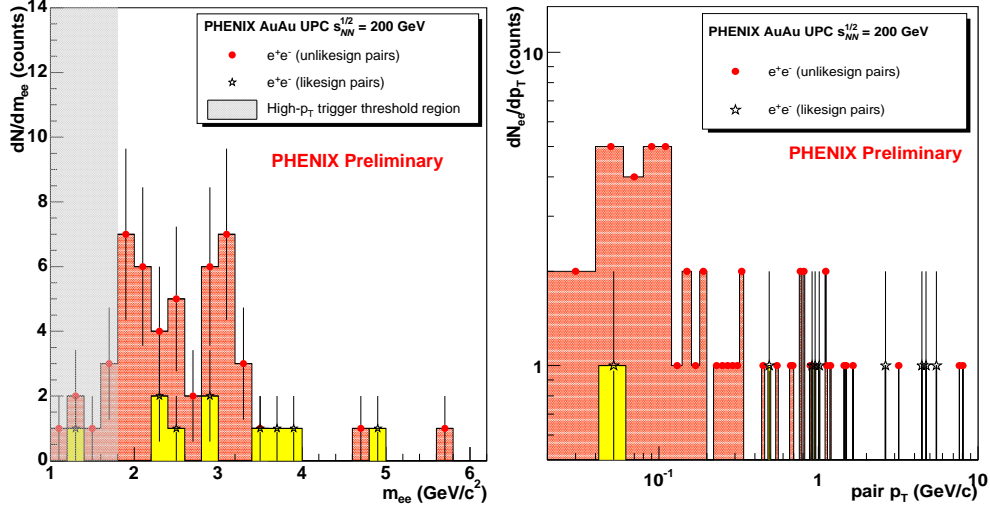

Fig. 5. Invariant mass (left) and pair p_T (right) distributions of unlike-sign (red dots) and like-sign (open stars) $e^{\pm}e^{\pm}$ pairs identified in UPC Au+Au collisions at $\sqrt{s_{NN}} = 200$ GeV.

3.1 Invariant mass distribution

The final measured background-subtracted dN/dm_{ee} distribution is shown in Fig. 6 including the simulated e^+e^- continuum power-law curve absolutely normalized at the measured dN/dm_{ee} yield at $m_{ee} = 2$ GeV/c^2 combined with a fit to a Gaussian at the J/ψ peak. The total number of counts for both physical signals is $N_{e^{\pm}+J/\psi} = 40 \pm 6$ (stat). Despite the poor statistics, the shape of the di-electron continuum is consistent with the power-law-like distribution expected for the reconstructed shape of the e^+e^- MC signal (Fig. 4). The dotted curves indicate the maximum and minimum e^+e^- continuum contributions that we consider in this preliminary analysis and have been obtained by absolutely normalizing the power-law curve at the upper and lower values given by the $\pm 1\sigma$ yield uncertainty at the $m_{ee} = 2.0$ GeV/c^2 bin. From this plot it is obvious that the largest contribution to the systematic uncertainty in the extraction of the J/ψ signal comes from the subtraction of this physical background.

Fig. 7 shows the resulting invariant mass distribution obtained by subtracting the fitted power-law curve of the dielectron continuum from the total experimental e^+e^- pairs distribution. There is a clear J/ψ peak whose position and width are perfectly consistent with the expected signal from our full MC: $m_{J/\psi} = 3.096 \pm 130$ MeV/c^2 (the mass is right at the PDG value, though the width seems to be $\sim$30 MeV/c^2 larger than the simulated value). The total number of J/ψ's within $\pm 3\sigma$ of the peak position (2.7 – 3.5 GeV/c^2) is: $N_{J/\psi} = 10 \pm 3$ (stat.) ± 3 (syst.), where the systematic uncertainty is completely dominated by the di-electron continuum subtraction method. More detailed analyses are being currently carried out to get a better handle on the possible $e^{\pm}$ continuum contamination to the total J/ψ signal.
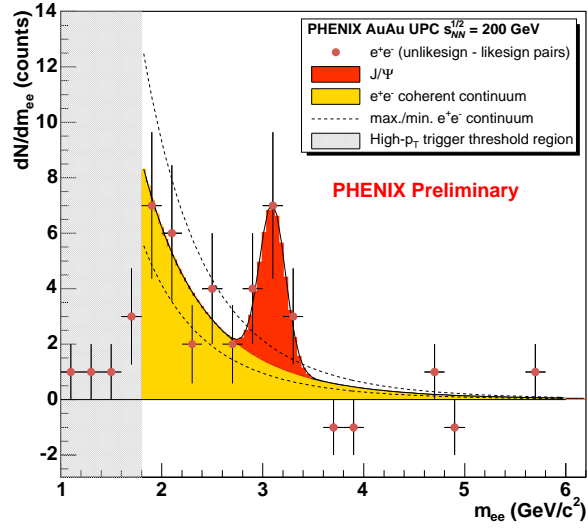
Fig. 6. Invariant mass distribution of e^+e^- pairs measured in UPC Au+Au collisions at $\sqrt{s_{NN}} = 200$ GeV fitted to the combination of a dielectron continuum (power-law distribution) and a J/ψ (Gaussian) signal. The two additional dashed curves indicate the maximum and minimum continuum contributions considered in this analysis below the J/ψ signal region.
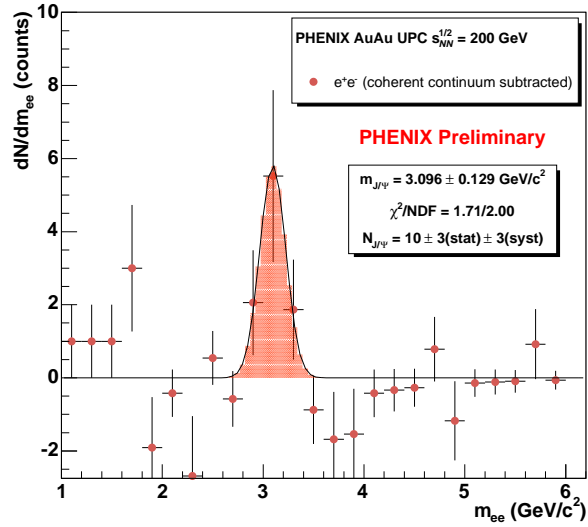

Fig. 7. J/ψ invariant mass distribution obtained subtracting from the total e^+e^- pairs signal the fitted dielectron continuum shown in Fig. 6. The quoted number of J/ψ is just the number of counts within m_{ee} = 2.7 – 3.5 GeV/c^2 (the error is just statistical).

3.2 Pair transverse momentum distribution

Fig. 8 shows the transverse momentum distribution of all the reconstructed e^+e^- continuum pairs and J/ψ in UPC Au+Au collisions. Their spectrum is clearly peaked at low p_T as expected for coherent production. The *shape* of the p_T spectrum itself is well reproduced by a nuclear form factor fit [43]

$$\frac{dN_{ee}}{dp_T} = C \cdot p_T \cdot |F(p_T)|^2 \quad \text{with} \quad F(p_T) = \frac{sin(R \cdot p_T) - R \cdot p_T \cdot cos(R \cdot p_T)}{(R \cdot p_T)^3 \cdot (1 + a_0^2 p_T^2)} \tag{10}$$

with Au nuclear radius and diffusivity fixed to their known values, $R = 6.38$ fm $a_0 = 0.54$ fm [44], and with absolute normalization factor C as the only free parameter.
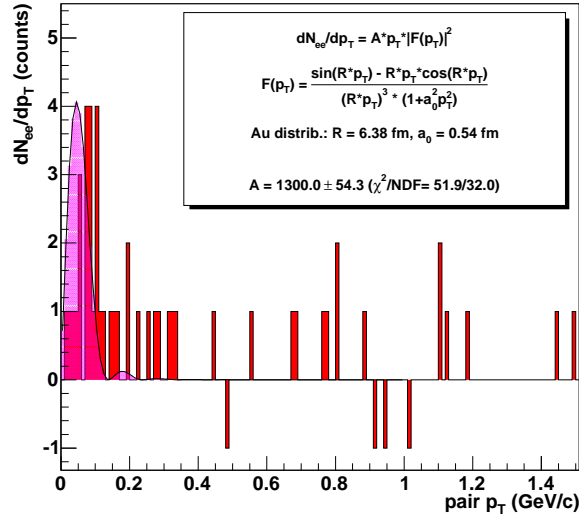

Fig. 8. Transverse momentum distribution of reconstructed e^+e^- continuum pairs and J/ψ from ultra-peripheral Au+Au collisions compared to the theoretical expectations of coherent photoproduction with a realistic nuclear form factor, Eq. (10).

3.3 Cross-section for coherent UPC J/ψ production at mid-rapidity

The final cross-section for coherent J/ψ photoproduction at midrapidity in UPC Au+Au collisions at $\sqrt{s_{NN}} = 200$ GeV accompanied by Au breakup is:

$$\frac{d\sigma_{UPC\,J/\psi}}{dy}\bigg|_{|y|<0.5} = \frac{1}{BR} \cdot \frac{N_{J/\psi}}{Acc \cdot \varepsilon_{reco} \cdot \varepsilon_{trigg} \cdot \mathcal{L}_{int}} \cdot \frac{1}{\Delta y} = 48. \pm 14.\,\text{(stat)} \pm 16.\,\text{(syst)}\,\mu b.$$

where all correction factors (and corresponding uncertainties) have been obtained as described in previous sections, and BR = 5.93% is the known J/ψ di-electron branching ratio. The final J/ψ cross-section is in very good agreement, within the (still large) experimental errors, with the theoretical values computed in [41, 22] as shown in Fig. 9 (the predictions of [22] have been scaled down by the nuclear breakup probability $P_{Xn} \sim 0.64$). The current uncertainties preclude yet any detailed conclusion regarding the two crucial ingredients of the models (nuclear gluon distribution and J/ψ nuclear absorption cross-section). Whereas the systematical uncertainty of the measurement is linked to the (yet) imprecise contribution from coherent $\gamma\gamma \rightarrow e^+e^-$ pairs

below the J/ψ peak, the statistical error can only be improved with a (much) higher luminosity Au+Au run. The contribution of the incoherent γN production to the total $d\sigma_{UPC\,J/\psi}/dy\big|_{|y|<0.5}$ (included in the predictions of Strikman *et al.* [22] but absent from *Starlight* [41]) needs to be elucidated too.
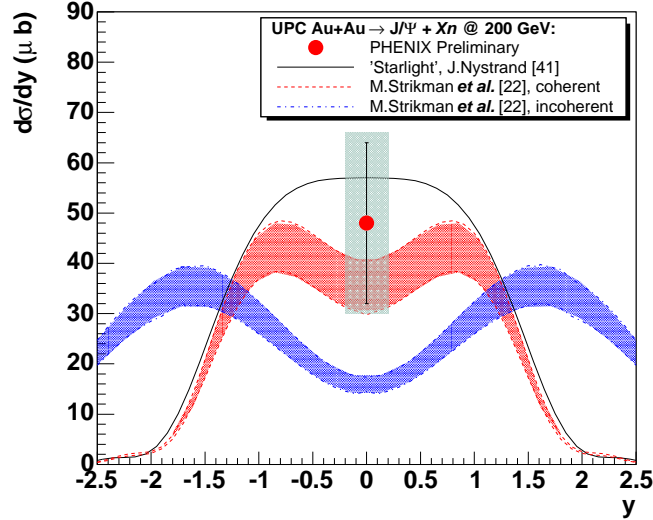

Fig. 9. Preliminary cross-section of coherent J/ψ production at mid-rapidity in UPC Au+Au collisions at $\sqrt{s_{NN}}$ = 200 GeV compared to the theoretical calculations [41,22]. The error bar (box) shows the statistical (systematical) uncertainties of the measurement.

4   CONCLUSION

We have presented preliminary PHENIX results from an analysis of Au+Au ($\sqrt{s_{NN}}$ = 200 GeV) UPC triggered events aiming at the measurement of coherent photoproduction of J/ψ and high-mass e^+e^- pairs in γA and $\gamma\gamma$ processes respectively. Ultraperipheral Au+Au collisions are tagged by forward (ZDC) neutron detection from the (single or double) Au* dissociation. Clear indications of J/ψ and high mass dielectron continuum have been found in the data. The total number of "physics" e^+e^- pairs is: $dN_{e^\pm+J/\psi}/dy = 40 \pm 6$ (stat). Their p_T spectrum is peaked at low $p_T \approx 90$ MeV/c as expected for coherent photoproduction with a realistic nuclear form factor. After subtraction of the physical e^+e^- signal, the measured invariant mass distribution has a clear peak at the J/ψ mass with experimental width in good agreement with a full GEANT-based simulation for UPC production and reconstruction in PHENIX. The measured number of J/ψ's in PHENIX acceptance is: $dN/dy = 10 \pm 3$ (stat) ± 3 (syst). After correcting for acceptance and efficiency losses and normalizing by the measured luminosity, we obtain a preliminary cross-section of $d\sigma/dy|_{y=0} = 48 \pm 16$ (stat) ± 18 (syst) μb which is consistent, within errors, with theoretical expectations. Foreseen improvements in our analysis will likely reduce the experimental uncertainties of the measured cross-section and provide more quantitative information on the nuclear gluon distribution and J/ψ absorption in cold nuclear matter at RHIC energies.

References

[1] V. M. Budnev, I. F. Ginzburg, G. V. Meledin and V. G. Serbo: *Phys. Rept.* **15** (1974) 181

[2] G. A. Schuler and T. Sjöstrand: *Nucl. Phys.* **B 407** (1993) 539

[3] A. Donnachie and P. V. Landshoff: *Phys. Lett.* **B 296** (1992) 227

[4] J. R. Cudell *et al.* [COMPETE Collaboration]: *Phys. Rev. Lett.* **89** (2002) 201801

[5] S. Eidelman *et al.* [Particle Data Group]: *Phys. Lett.* **B 592** (2004) 1

[6] C.F. Weizsäcker: *Z. Phys.* **C 88** (34) 612 ; E.J. Williams: *Phys. Rev.* **45** (34) 729

[7] See e.g. J. M. Butterworth and M. Wing: *Rept. Prog. Phys.* **68** (2005) 2773

[8] R. Engel: *Z. Phys.* **C 66** (1995) 203

[9] T. H. Bauer, R. D. Spital, D. R. Yennie and F. M. Pipkin: *Rev. Mod. Phys.* **50** (1978) 261

[10] See e.g. M. Klasen: *Rev. Mod. Phys.* **74** (2002) 1221

[11] See e.g. P. Aurenche, M. Fontannaz and J. P. Guillet: *Eur. Phys. J.* **C 44** (2005) 395

[12] H. Kowalski and D. Teaney: *Phys. Rev.* **D 68** (2003) 114005

[13] V. P. Goncalves and M. V. T. Machado: *Eur. Phys. J.* **C 40** (2005) 519; also hep-ph/0506331

[14] R. Engel and J. Ranft: *Phys. Rev.* **D 54** (1996) 4244

[15] A. De Roeck: *Nucl. Phys. Proc. Suppl.* **126** (2004) 386

[16] S. R. Klein and J. Nystrand: *Phys. Rev. Lett.* **92** (2004) 142003

[17] G. Baur, K. Hencken and D. Trautmann: *J. Phys* **G 24** (1998) 1657

[18] G. Baur, K. Hencken, D. Trautmann, S. Sadovsky and Y. Kharlov: *Phys. Rept.* **364** (2002) 359

[19] C. A. Bertulani, S. R. Klein and J. Nystrand: *Ann. Rev. Nucl. Part. Sci.* **55** (2005) 271

[20] J. D. Jackson: *Classical Electrodynamics*, 2nd edition, John Wiley&Sons, 1975

[21] L. Frankfurt, W. Koepf and M. Strikman: *Phys. Rev.* **D 54** (1996) 3194

[22] M. Strikman, M. Tverskoy and M. Zhalov: *Phys. Lett.* **B 626** (2005) 72

[23] M. G. Ryskin, R. G. Roberts, A. D. Martin and E. M. Levin: *Z. Phys.* **C 76** (1997) 231

[24] A. J. Baltz: *Phys. Rev.* **C 71** (2005) 024901 [Erratum-ibid. **71** (2005) 039901]

[25] C. A. Bertulani and G. Baur: *Phys. Rept.* **163** (1988) 299

[26] S. R. Klein, J. Nystrand: *Phys. Rev.* **C 60** (1999) 014903

[27] A. J. Baltz, S. R. Klein, J. Nystrand: *Phys. Rev. Lett.* **89** (2002) 012301

[28] C. Adler *et al.* [STAR Collaboration]: *Phys. Rev. Lett.* **89** (2002) 272302

[29] J. Adams *et al.* [STAR Collaboration]: *Phys. Rev.* **C 70** (2004) 031902

[30] G. Baur, K. Hencken, A. Aste, D. Trautmann and S. R. Klein: *Nucl. Phys.* **A 729** (2003) 787 .

[31] W. Fischer *et al.*: EPAC-2004-MOPLT165, EPAC 2004, Lucerne, Switzerland, 5-9 Jul 2004.

[32] K. Adcox *et al.* [PHENIX Collaboration]: *Nucl. Instrum. Meth.* **A 499** (2003) 469

[33] L. Aphecetche *et al.* [PHENIX Collaboration]: *Nucl. Instrum. Methods* **499** (2003) 521

[34] C. Adler *et al.*: *Nucl. Instrum. Meth.* **A 470** (2001) 488

[35] M. Chiu, A. Denisov, E. Garcia, J. Katzy and S. White: *Phys. Rev. Lett.* **89** (2002) 012302

[36] S.S. Adler *et al.* [PHENIX Collaboration]: *Phys. Rev. Lett.* **91** (2003) 072301

[37] R. Engel, M. A. Braun, C. Pajares and J. Ranft: *Z. Phys.* **C 74** (1997) 687

[38] C. G. Roldao and A. A. Natale: *Phys. Rev.* **C 61** (2000) 064907

[39] J. Mitchell *et al.*: *Nucl. Instrum. Methods* **A482** (2002) 491

[40] S. S. Adler *et al.* [PHENIX Collaboration]: *Phys. Rev.* **C 69** (2004) 014901

[41] J. Nystrand: *Nucl. Phys.* **A 752** (2005) 470c

[42] GEANT 3.21: CERN program library

[43] J. Nystrand: nucl-th/0112055

[44] B. Hahn, D.G. Ravenhall and R. Hofstadter: *Phys. Rev.* **101** (1956) 1131